JOURNAL OF GUIDANCE, CONTROL, AND DYNAMICS
Vol. 32, No. 5, September–October 2009

Design of Robust Drag-Free Controllers with Given Structure

Lorenzo Pettazzi*
University of Bremen, 28359 Bremen, Germany
Alexander Lanzon†
University of Manchester, Manchester, England M60 1QD, United Kingdom
Stephan Theil‡
DLR, German Aerospace Center, 28359 Bremen, Germany
and
Amalia Ercoli Finzi§
Politecnico di Milano, 20156 Milano, Italy

DOI: 10.2514/1.40279

In this paper the problem of designing a robust controller with given structure for a plant describing a drag-free satellite is addressed. From recent experiences in drag-free control design we first derive an uncertain plant set representative of many drag-free missions with nonspherical test masses. The design plant is uncertain and a performance requirement is imposed on the absolute acceleration of the test mass along a measurement axis. The ν-gap metric is first used to derive a simplified uncertain design plant. Then the main performance requirement is broken down into requirements on the uncertain closed loop behavior of the simplified system. The fulfillment of this new set of requirements guarantees robust achievement of the overall system goal. Then optimal single-input–single-output controllers are designed that robustly achieve the desired level of performance. The method proposed allows one to properly account for the uncertainties in the system retaining the decentralized structure of the controller suggested by the peculiar features of the design plant.

I. Introduction

IN RECENT years many space missions have demonstrated that high performance in space in terms of spacecraft positioning and attitude acquisition and maintenance can be achieved by the current technology. On the basis of these achievements space has recently been considered for high precision physics experiments such as the ones involving measurements of gravitational waves and relativistic effects (LISA Pathfinder [1], LISA [2], Microscope [3], STEP [4]).

In all these missions the drag-free satellite concept [5] plays a key role. The drag-free satellite contains a cavity in which a test mass (or proof mass) is let free to fly. The test mass is shielded by the surrounding spacecraft against the disturbances acting on the surface so that its motion is influenced only by the gravitational force and by the small gravitational and electrostatic interaction existing with the spacecraft. Both these contributions show spatial dependence so that a stiffnesslike interaction exists between the proof mass and the spacecraft [1]. The accuracy level of the free fall trajectory followed by the test mass depends therefore on the capability of the control system to keep the test mass at the center of the cavity. The free fall requirements are usually specified as acceleration spectral noise densities along a specific axis that is the sensitive axis of the experiment. The control is actuated with high precision continuous thrusters so that the spacecraft is forced to chase the test mass in its purely gravitational motion at least along the sensitive axis. However, for nonspherical proof masses or if more than one test mass is present onboard, an electrostatic suspension actuator must be included to control the relative attitude of the test mass with respect to the spacecraft.

The requirements imposed by the scientific goal imply challenging design tasks to be achieved both at a system level and from a control synthesis point of view. From the system design point of view, the main objective is to reduce as much as possible the dynamic couplings between the spacecraft and the test mass. On the other hand, the control synthesis is aimed at stabilizing the relative motion of the test mass with respect to the spacecraft and to provide the required level of disturbance rejection. In this paper only the controller synthesis problem is addressed.

In many past investigations [1,6–9] it is assumed that the overall system is designed so that the couplings among the different degrees of freedom are highly reduced. This allows one to tackle the control design procedure as a synthesis of a set of single-input/single-output (SISO) controllers completely ignoring the coupling effects. Then, simple proportional–integral–derivative design methods [6], an optimization approach based on the definition of penalty functions [7,10] and $\mathcal{H}_\infty$ synthesis techniques [1,9], have been proposed as methods to synthesize the SISO controllers. In all these cases no structured uncertainty is considered in the design plant so that the achievement of the top level performance requirement of the whole system in the presence of perturbations must be checked a posteriori.

In this paper the problem of designing a decentralized robust controller for a plant describing a drag-free satellite is addressed in a more systematic way. To better illustrate the controller design technique, a 2-degree-of-freedom design plant representative of the most modern drag-free satellites [10,11] is first defined. Then a two-stage design technique is proposed. In the first phase the structure of the plant and the measurement relation are exploited to derive bounds on the individual closed loop responses, that, when satisfied, guarantee the robust performance of the overall system. In the second phase a recently developed control design technique [12] based on the mixed structured singular value is used to synthesize SISO controllers that robustly achieve the performance specified by the individual bounds. The proposed synthesis technique automatically

Received 7 August 2008; revision received 18 April 2009; accepted for publication 1 May 2009.

*Currently Development Engineer, LFK-Lenkflugkörpersysteme GmbH, Flight Control/Systems and Realtime Simulation, OPS3 Landshuter Straße 26, 85716 Unterschleissheim, Germany; lorenzo.pettazzi@mbda-systems.de.

†Lecturer, Control Systems Centre, School of Electrical and Electronic Engineering, Sackville Street. Member AIAA.

‡Head of Control and Simulation Department, Institute of Space Systems, Robert-Hooke-Strasse 7. Member AIAA.

§Full Professor, Department of Aerospace Engineering, Campus Bovisa Sud via La Masa 34. Member AIAA.

performs an optimized tradeoff between achievable performance and limitations due to uncertainty or plant dynamics for the SISO plants verifying if the performance requirements derived in the previous step may be achieved. Finally, to validate in a more realistic scenario the results of this paper, controllers derived with the technique developed in this work are implemented and tested in a nonlinear simulation scenario.

The benefit associated with this methodology is twofold. From one side it allows for the direct design of a decentralized controller that automatically achieves robust performance without requiring any a posteriori analysis. On the other hand, for a given design plant model with an associated level of uncertainty, it helps to assess if the overall system goal is achievable by independent controller designs. As a final remark, note that the discretization of the designed control law is not directly addressed in the present paper. However, the method presented in this paper indeed yields controllers that are suitable for a digital implementation and it can thus be used in connection with state of the art controller discretization techniques. The use of discretization techniques for the digital implementation of drag-free controllers designed with frequency shaping methods is presented, for example, in [7]. A completely different approach is described in [13], where the problem of designing a drag-free controller is tackled directly in the discrete time domain. A discussion about the advantages and the drawbacks of controller discretization versus direct design of digital controllers can be found in [14].

The notation used throughout the paper is introduced as follows: Let $\bar{\mathbb{R}}_+$ denote the nonnegative real numbers, $\bar{\mathbb{C}}_+$ denote the closed right half complex plane, and $\mathbb{C}^{m\times n}$ denote complex matrices of dimension $m \times n$. The maximum singular value of a matrix $A \in \mathbb{C}^{m\times n}$ is denoted by $\bar{\sigma}(A)$. A^T (respectively, A^*) is the transpose (respectively, complex conjugate transpose) of $A \in \mathbb{C}^{m\times n}$ and $\|A\|_F$ denotes the Frobenius norm of the matrix A. The $k \times k$ identity matrix and zero matrix are denoted by I_k and O_k, respectively, whereas E_k denotes a $k \times k$ matrix fully padded with ones. $\otimes$ denotes the Kronecker product. A real rational matrix function $\Gamma(s)$ of a complex variable s is such that $\Gamma(s) \in \mathcal{RH}_\infty$ if it is bounded and analytic in the open complex right half-plane. The adjoint system of $\Gamma(s)$ is defined by $\Gamma^\sim(s) = \Gamma(-s)^T$. The $\|\cdot\|_\infty$ norm of a $m \times n$ matrix function $\Gamma(s)$ is defined by $\|\Gamma\|_\infty := \sup_\omega \bar{\sigma}(\Gamma(j\omega))$. Finally, $\mathrm{diag}_{i=1}^N(A_i)$ with $A_i \in \mathbb{C}^{m_i\times n_i}$, $i = 1, \ldots, N$ denotes the $\sum_i m_i \times \sum_i n_i$ block diagonal complex matrix composed of A_i, $i = 1, \ldots, N$.

II. Plant Model

In Fig. 1, the drag-free satellite layout is sketched and the reference frames used for the definition of the equations of motion are displayed. In this figure Σ_I denotes the geocentric reference frame, Σ_{SC} the spacecraft body reference frame, and Σ_{TM} is the reference frame attached to the test mass. The satellite can be divided in two different subsystems, the spacecraft and the experiment on board. The experiment includes a cavity (or housing) that contains a partially free flying proof mass. Position and attitude of the test mass with respect to the spacecraft are measured by means of an electrostatic sensor. The main control objective is to minimize the acceleration noise density on the test mass along some sensitive axis. To this end, in the direction of the sensitive axis high precision field emission electric propulsion (FEEP) thrusters are used to control the position of the satellite such that the proof mass remains in the center of the cavity. Moreover, to ensure a proper communication link with the ground station or a proper thermal conditioning, a requirement is usually imposed on the absolute attitude of the satellite. This control task is achieved feeding back the measurement from the star tracker by means of the FEEP thrusters. A suspension actuation system is then required to align the test mass attitude to the one of the satellite [9].

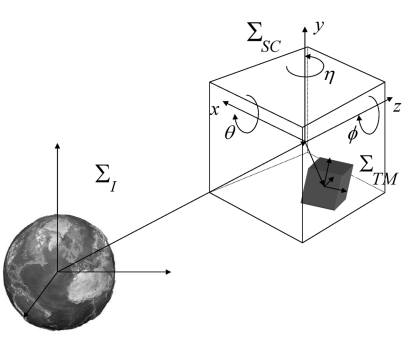

Fig. 1 Schematic view of drag-free satellite.

In this paper the attitude of the satellite is controlled with an independent feedback loop with respect to the test mass relative position. The remainder of this paper is focused on the derivation of the controllers for the test mass relative position and attitude. The design of the attitude control for the spacecraft is therefore assumed and is not included in the present paper.

A. System Dynamics

In this section the linearized equations describing the motion of Σ_{TM} with respect to Σ_{SC} are derived. In particular, the simplified model in this paper considers only the displacement along the spacecraft x body axis and the rotation ϕ around the spacecraft z body axis. However, the control design technique developed here can be easily applied to more complex dynamic models as demonstrated in Sec. VI and in [15]. The set of linearized equations describing the relative motion of the test mass with respect to the spacecraft is [10]

$$\ddot{q} = M_q^{-1}[f_e + f_{\exp} + f_h + M_u \ddot{q}_{\mathrm{SC}}] \tag{1}$$

where $q = [x, \phi]^T$, $M_q = \mathrm{diag}(m_{\mathrm{TM}}, I_{\mathrm{TM}})$ represents the proof mass generalized mass matrix (mass plus inertia), M_u is the sensitivity of the test mass dynamics to the spacecraft linear ($\ddot{x}_{\mathrm{SC}}$) and angular ($\ddot{\phi}_{\mathrm{SC}}$) acceleration, expressed in the vector $\ddot{q}_{\mathrm{SC}}$. The generalized forces (forces and torques) acting on the test mass are divided into three contributions f_e, $f_{\exp}$, and f_h. A brief description of the three terms is presented as follows:

1) f_e are the external generalized forces acting on the test mass: this contribution is mainly due to the interplanetary gravitational and magnetic fields acting directly on the test mass.

2) $f_{\exp}$ are the generalized forces acting between test mass and the experiment: this contribution is mainly due to gravitational, electrostatic, and magnetic interactions between the spacecraft and the test mass.

3) f_h are the generalized forces acting between electrode housing and the test mass: these are mainly electrostatic forces due to the suspension control loop.

Both $f_{\exp}$ and f_h show spatial dependence so that it is convenient to represent them by means of a series expansion:

$$f_h = f_{h_0} + f_{\mathrm{SUS}} + K_h q \tag{2}$$

$$f_{\exp} = f_{\exp_0} + K_{\exp} q \tag{3}$$

where f_{SUS} are the electrostatic suspension generalized forces acting on the test mass and $K_{\exp} := \partial f_{\mathrm{ext}}/\partial q$ and $K_h := \partial f_h/\partial q$ are the corresponding stiffness matrices. Moreover, a direct cross talk is included in the electrostatic actuation. The relation between the commanded suspension forces F_{SUS} and the real ones f_{SUS} can be expressed by

$$f_{\mathrm{SUS}} = (I + H_{IS}) F_{\mathrm{SUS}}$$

where H_{IS} is the actuation cross-talk matrix.

The linearized equation of motion of the spacecraft is

$$\ddot{q}_{\mathrm{SC}} = M_{\mathrm{SC}}^{-1}[f_{\mathrm{SC}} + f_{\mathrm{dist}} + f_{\mathrm{DF}}] \tag{4}$$

where M_{SC} is the spacecraft generalized mass matrix, f_{dist} is the external disturbance acting on the spacecraft, and f_{SC} is the total generalized force between the spacecraft and the experiment.

Assuming that the satellite is placed in a low disturbance environment, for example, in the Earth–sun Lagrangian point [7], the main contributions to the disturbance force acting on the satellite are thruster noise and solar radiation drag. f_{DF} contains the force and torque acting on the spacecraft due to the drag-free control. This action is provided by means of FEEP thrusters, modeled here as a first-order system with a characteristic time constant of 0.1303 s (corresponding to approximately 0.3 s rise time). The selected time constant takes into account the delays introduced by the electronic devices driving the thrusting actuators [16,17]. In this paper the FEEP thrusters are considered as a baseline actuator system because they have been identified as a key technology for future drag-free missions [17]. However, other technologies such as colloidal micronewton thrusters [18] or ion thrusters [13] are currently taken into consideration in the development of drag-free missions.

In a typical configuration the mass of the spacecraft is approximately 2 orders of magnitude larger than the one of the test mass. Therefore, the force balance on the spacecraft is dominated by the thrusters effect and the solar radiation pressure so that the term f_{SC} in Eq. (4) can be neglected. Substituting Eqs. (2) and (3) into Eq. (1) and neglecting f_{SC} in Eq. (4) yields the following expression:

$$\ddot{q} = M_q^{-1}\{Kq + f_{\mathrm{SUS}} + f_{\mathrm{TM}} + (M_u M_{\mathrm{SC}}^{-1})(f_{\mathrm{dist}} + f_{\mathrm{DF}})\} \tag{5}$$

where $K = K_{\mathrm{exp}} + K_h$ and $f_{\mathrm{TM}} = f_{h_0} + f_{\mathrm{exp}_0} + f_e$ is the disturbance force directly acting on the proof mass. The numerical values of the physical characteristics of the system are displayed in Table 1 and are consistent with the ones in [19,20] describing a similar system. Note that the stiffness values displayed in Table 1 will result in an unstable behavior of the design plant.

To translate the science objective into controller requirements the measurement equation must be derived. In the example considered in this paper, a performance requirement is imposed on the residual absolute acceleration along the x axis. This can be expressed as a function of the noises on the coordinates x and ϕ and of the suspension actuation and disturbance forces acting upon the test mass as

$$y = m_{\mathrm{TM}}^{-1}[f_{\mathrm{TM}_x} + h_{IS}F_{\mathrm{SUS}_\phi} + K_{xx}x + K_{x\phi}\phi] \tag{6}$$

Finally, the controller sampling rate is set to 10 Hz whereas it is assumed that the typical experiment time during the mission is 10^5 s. These values are again consistent with those used for missions currently under development (see, for example, [7,10]).

B. System Disturbances

The input disturbances acting on the test mass are mainly due to spacecraft/test mass gravitational and electrostatic interactions. In this work the total stray force acting on the test mass is assumed to be dominated by electrostatic contribution. The weighting functions used in this paper to model the frequency content of f_{TM} are consistent with the ones in [20].

On the other hand, the disturbances acting on the spacecraft are mainly due to the noise associated with the FEEP thrusters and the solar radiation pressure. According to the work in [20], they have been modeled as zero-mean Gaussian white noise shaped by a low pass filter. The filters used to describe the different input disturbances

Table 1 Numerical data of the drag-free satellite

Parameter	Numerical value
m_{SC}	500 kg
I_{SC}	500 kg · m^2
m_{TM}	1 kg
I_{TM}	6×10^{-4} kg · m^2
$K := \begin{bmatrix} K_{xx} & K_{x\phi} \\ K_{\phi x} & K_{\phi\phi} \end{bmatrix}$	$\begin{bmatrix} 2 \times 10^{-6}\ \frac{\mathrm{N}}{\mathrm{m}} & 0.003 \times 10^{-6}\ \frac{\mathrm{N}}{\mathrm{rad}} \\ 0.006 \times 10^{-6}\ \mathrm{N} & 0.004 \times 10^{-6}\ \frac{\mathrm{N \cdot m}}{\mathrm{rad}} \end{bmatrix}$
$H_{IS} := \begin{bmatrix} 0 & h_{IS} \\ 0 & 0 \end{bmatrix}$	$\begin{bmatrix} 0 & 0.5\ \frac{1}{\mathrm{m}} \\ 0 & 0 \end{bmatrix}$

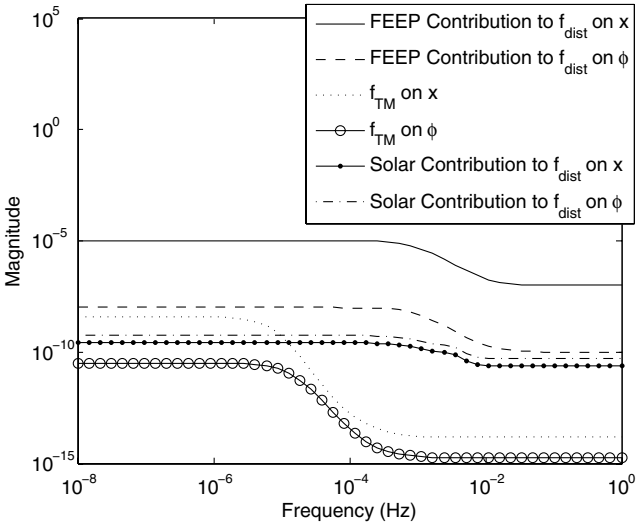

Fig. 2 Input disturbances weights. Units for disturbance on x are $\mathrm{N}/\sqrt{(\mathrm{Hz})}$, and on ϕ are $\mathrm{N \cdot m}/\sqrt{(\mathrm{Hz})}$.

are displayed in Fig. 2. The solar noise power spectral density (PSD) has been derived taking into account the measurements performed by the VIRGO (Variability of solar Irradiance and Gravity Oscillations) experiment onboard the SOHO (Solar and Heliospheric Observatory) mission (see again [20]). The suspension actuation noise weighting function has been defined assuming a torque resolution of 1.52×10^{-15} N · m (corresponding to a maximum electrostatic force [21] of 2.5×10^{-9} N and considering a 16 bits converter between the controller and the suspension actuator [22]). Similarly, the FEEP actuation noise PSD takes into account the equivalent quantization noise associated to thrusters with 0.1 μN thrust resolution [17]. Moreover, the external disturbance due to the FEEP thruster acting on the ϕ axis is assumed 10^3 times smaller with respect to the one acting on the x axis. This allows one to take into account the disturbance reduction behavior of the attitude controller of the spacecraft, not included in the present model. However, this assumption is removed in the simulation performed with the nonlinear simulator given in Sec. VI. As a final remark, note that the noise due to the FEEP thrusters and the solar radiation drag are the dominant contributions in the frequency range between 10^{-5} and 10 Hz on both the x and on the ϕ axes. This justifies the assumption made by neglecting f_{SC} in the derivation of Eq. (5).

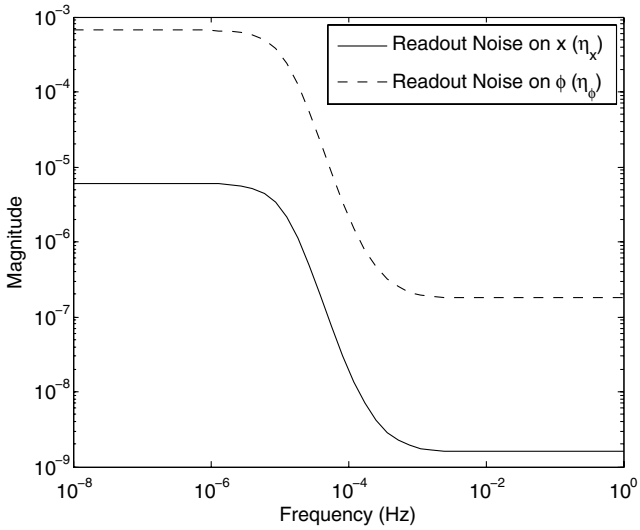

Fig. 3 Readout disturbances weights. Units for disturbance on x are $\mathrm{m}/\sqrt{(\mathrm{Hz})}$, and on ϕ are $\mathrm{rad}/\sqrt{(\mathrm{Hz})}$.

The noise associated with the measurement process is also modeled as zero-mean Gaussian white noise preshaped with a low pass filter. The magnitude plots for the readout noise filters are consistent with the ones in [20] and are shown in Fig. 3.

C. Uncertainty Model

The design of a robustly performing controller first requires the definition of a mathematical model with associated uncertainty models. The main source of uncertainty for the scientific drag-free missions is the instrument itself. Even small imperfections in the design of the instrument may cause nonnegligible perturbations on the test mass motion resulting in the loss of performance of the whole system [9]. The force interaction between the spacecraft and the test mass is modeled as a stiffness coupling defined by means of the matrix K and by the electrostatic cross coupling h_{IS}. These interactions are very difficult to model on ground and therefore on-orbit calibration experiments, that shall allow one to estimate these parameters before the spacecraft starts collecting science measurements, are currently under investigation [21]. Therefore, an uncertainty of $\pm 50\%$ with respect to the nominal value listed in Table 1 is considered on each entry of the stiffness matrix and on the electrostatic cross coupling h_{IS}. A reference for the selected uncertainty values can be found, for example, in [7,23].

The FEEP thrusters are the second source of uncertainty in the system. This technology is still under development and therefore a certain level of uncertainty must be considered in the dynamical model representing the actuator. Following the results in [16] the FEEP thruster is modeled here as a first-order system, that is,

$$\Gamma_{\text{FEEP}} = \frac{\kappa_{\text{FEEP}}}{1 + \tau s}$$

An uncertainty of $\pm 5\%$ on the scale factor κ_{FEEP} takes into account the undetermined static behavior of the thruster. On the other hand, measurements of the real dynamic behavior of the system have shown that the time constant τ depends on the current thrust value and on the amount of thrust variation. For this reason an uncertainty of $\pm 50\%$ is considered on the FEEP time constant.

The block diagram representing the system described in this section is shown in Fig. 4a where the following definitions hold:

$$\Gamma = \begin{bmatrix} \Gamma_{xx} & \Gamma_{x\phi} \\ \Gamma_{\phi x} & \Gamma_{\phi\phi} \end{bmatrix} := \frac{1}{\det(s^2 I - M_q^{-1} K)} \begin{bmatrix} s^2 - \frac{K_{\phi\phi}}{I_{\text{TM}}} & \frac{K_{x\phi}}{m_{\text{TM}}} \\ \frac{K_{\phi x}}{I_{\text{TM}}} & s^2 - \frac{K_{xx}}{m_{\text{TM}}} \end{bmatrix}$$

and where d_{SC} and d_{TM} denote the exogenous disturbance per unit mass/inertia acting, respectively, on the spacecraft and the test mass whereas η_x and η_ϕ denote the sensor readout noise on the x and ϕ axes, respectively. The FEEP model is included in the plant and the different noise sources are considered as they naturally appear in the loop. Two control blocks are included in this scheme: one commanding the FEEP actuator (K_{DF}) and one commanding the electrostatic actuation (K_{SUS}). Uncertainties appear in the plant describing the drag-free satellite dynamics as well as in the FEEP model.

III. Derivation of Specifications for Decentralized Control Design

In this work the control design will be considered successful if the residual absolute acceleration acting on the test mass along the x direction is kept below

$$\mathcal{S}_y^{1/2} \leq 2 \times 10^{-14} \left[1 + \left(\frac{f}{3\ \text{mHz}} \right)^2 \right] \frac{\text{m}}{\text{s}^2} \frac{1}{\sqrt{\text{Hz}}} \tag{7}$$

in the measurement bandwidth (MBW)

$$1\ \text{mHz} \leq f \leq 30\ \text{mHz}$$

in the presence of uncertainty as defined in the previous section. This requirement represents the technological goal of missions currently under development [1] and therefore it will be taken here as reference. Moreover, a decentralized controller structure is assumed in this work where the test mass x position is fed back by means of the thruster actuation and the attitude error is fed back by means of the suspension actuation. This situation is encountered when the requirement of Eq. (7) must be satisfied together with a requirement on the orientation of the spacecraft. Being the main science objective to reduce the residual action on the test mass along the x direction, the choice to control the test mass x position with the thruster is highly recommended. The constraint imposed on the controller structure does not allow, in principle, the application of the classical μ-synthesis technique ($D - K$ iteration) to the multi-input/multi-output (MIMO) system. An attractive alternative solution is to break down the nearly diagonal uncertain plant into two different SISO plants neglecting in the definition of the uncertain plant set the off-diagonal elements of the stiffness matrix and h_{IS}. However, by considering the stiffness and the cross-coupling matrices as diagonal we are, in fact, doing an approximation of the set of uncertain design plants Γ. To get insight about the level of approximation introduced, we measure the distance between the original uncertain plant set Γ and the approximated one, denoted here by Γ_d, exploiting the ν-gap metric [24]. The ν-gap metric has been introduced to define a notion of distance in the space of possibly unstable linear time invariant (LTI) systems. In particular, the ν gap between two different LTI systems not affected by uncertainty provides an indication of how close the responses of the two systems are under the same feedback. If the ν gap between two systems is small, then it is reasonable to expect that any controller that will work well in terms of robust performance for one plant will work well also for the other. The ν-gap metric has been considered in this work to first introduce the definition of approximation to a given accuracy of an uncertain plant set.

Definition 1: Let $\tilde{\Gamma}$ and $\tilde{\Gamma}_d$ be any perturbed plant belonging to the uncertain plant sets Γ and Γ_d, respectively, and let $\delta_t \in [0, 1]$. Then Γ_d is said to be an approximation of Γ of accuracy δ_t if the following two conditions hold:

$$\forall\ \tilde{\Gamma} \in \Gamma, \quad \exists\ \tilde{\Gamma}_d \in \Gamma_d \quad \text{such that } \delta_v(\tilde{\Gamma}, \tilde{\Gamma}_d) \leq \delta_t \tag{8}$$

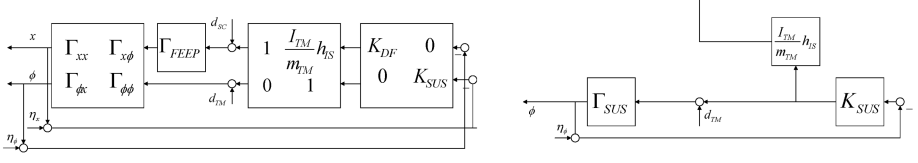

a) Coupled MIMO block diagram of the drag-free satellite system

b) Decoupled MIMO block diagram of the drag-free satellite system

Fig. 4 Multi-input/multi-output system block diagram representation.

$$\forall\ \tilde{\Gamma}_d \in \Gamma_d, \quad \exists\ \tilde{\Gamma} \in \Gamma \quad \text{such that } \delta_v(\tilde{\Gamma}, \tilde{\Gamma}_d) \le \delta_t \tag{9}$$

Observe that, if $\Gamma_d \subset \Gamma$, then Eq. (8) $\Rightarrow$ Eq. (9). The conditions in Eqs. (8) and (9) are verified if and only if the following holds:

$$\sup_{\tilde{\Gamma}\in\Gamma} \inf_{\tilde{\Gamma}_d\in\Gamma_d} \delta_v(\tilde{\Gamma}, \tilde{\Gamma}_d) \le \delta_t \tag{10}$$

$$\sup_{\tilde{\Gamma}_d\in\Gamma_d} \inf_{\tilde{\Gamma}\in\Gamma} \delta_v(\tilde{\Gamma}, \tilde{\Gamma}_d) \le \delta_t \tag{11}$$

In this work the minimum δ_t satisfying the inequalities in Eqs. (10) and (11) is computed by performing a direct search over the discretized space of uncertain parameters.

Moreover, to separately assess the importance of the different parameters, the approximation introduced by neglecting the off-diagonal elements of the stiffness matrix and h_{IS} has been measured performing two different analyses, whose results are shown in Table 2. From this table it is possible to conclude that, with the current model, the off-diagonal elements of the stiffness matrix can be neglected, whereas the electrostatic actuation cross coupling cannot. Note that considering the interpretation of the ν-gap metric in frequency domain [24], it is also possible to define a frequency dependent distance measure $\delta_t(\omega)$ that may also allow identification of the frequency regions where a given uncertainty dominates. However, such a detailed analysis is not necessary in the simple example considered in this work and therefore is not included here for the sake of conciseness.

The resulting simplified plant is therefore the one shown in Fig. 4b where the following definitions hold:

$$\Gamma_{\mathrm{DF}} = \frac{1}{s^2 - (K_{xx}/m_{\mathrm{TM}})}\Gamma_{\mathrm{FEEP}} \qquad \Gamma_{\mathrm{SUS}} = \frac{1}{s^2 - (K_{\phi\phi}/I_{\mathrm{TM}})}$$

Because in the current design plant the h_{IS} parameter is uncertain, it is not possible to cancel out the undesired electrostatic force on the test mass by taking into account h_{IS} in the definition of the suspension control law. However, even assuming a perfect knowledge of h_{IS}, the inversion of the direct cross-coupling matrix in the definition of the control law is not always desirable because it requires the application of a direct force on the test mass along the measurement axis. This may lead to an increase in the stiffness coupling between the spacecraft and the test mass along the x axis resulting in more stringent requirements on the test mass's jitter. For these reasons the electrostatic cross coupling is treated here as an additional input disturbance to be rejected by the drag-free loop. Moreover, the resulting system is diagonal dominant. Therefore, a decentralized controller that stabilizes the diagonal plant stabilizes the nondiagonal plant as well. If the controller task is only to stabilize the system, the cross-coupling term can be neglected. However, h_{IS} together with the off-diagonal elements of K appear also in the measurement equation. Therefore, an uncertainty on these parameters may still be critical for the achievement of the top level requirement and must be properly accounted for. To this end, we write the closed loop expression of both the two individual loops and we substitute it into Eq. (6) to obtain an approximation of the closed loop measurement equation

Table 2 Results of ν-gap analysis

Neglected parameters	δ_t
$K_{x\phi}$, $K_{\phi x}$	0.0054
h_{IS}	0.6

where the standard notation is used for the sensitivity and complementary sensitivity functions

$$S_{\mathrm{DF}} = (1 + K_{\mathrm{DF}}\Gamma_{\mathrm{DF}})^{-1} \qquad T_{\mathrm{DF}} = K_{\mathrm{DF}}\Gamma_{\mathrm{DF}}(1 + K_{\mathrm{DF}}\Gamma_{\mathrm{DF}})^{-1}$$
$$S_{\mathrm{SUS}} = (1 + K_{\mathrm{SUS}}\Gamma_{\mathrm{SUS}})^{-1}$$
$$T_{\mathrm{SUS}} = K_{\mathrm{SUS}}\Gamma_{\mathrm{SUS}}(1 + K_{\mathrm{SUS}}\Gamma_{\mathrm{SUS}})^{-1}$$

If structured uncertainties are not to be considered explicitly in the design, the closed loop individual functions can be shaped via an $\mathcal{H}_\infty$ loop shaping technique, for example, from the knowledge of the nominal values of the stiffness parameters and the actuation cross talk [20]. On the other hand, a design that aims at maximizing the tolerable parametric uncertainties appearing in the SISO closed loop functions can be performed by means of the classical $D-K$ iteration. This approach requires the definition of performance weights in order to shape the design of the individual controllers toward the achievement of the requirement in Eq. (7). However, the definition of appropriate weighting functions is by no means a trivial task and it is often the result of a tedious trial and error procedure. In this paper the measurement equation in Eq. (12) is used to break down the requirements in Eq. (7) into independent requirements on the closed loop behavior of the drag-free and suspension loops. The fulfillment of these requirements is a sufficient condition of robust performance of the overall system. Then a novel control design technique [12] is used to synthesize optimized performance weights and controller together into one algorithm in a systematic way. The synthesis algorithm involves the iterative solution of an optimization problem aimed at maximizing the size of the performance weights in certain directions to achieve desired specifications. This optimization is restricted by the constraint that there exists an internally stabilizing controller that achieves robust performance with respect to the maximized weights. The designer is only required to specify the plant uncertain set and some frequency dependent functions, dubbed optimization directionalities, that reflect, in a qualitative way, the desired performance requirements over all frequency. The specification of the optimization directionality functions is easier than the direct design of the performance weights and can be easily derived by the information about the way the different exogenous disturbances enter in the performance cost in Eq. (12).

IV. Control Synthesis Technique

In this work the optimization based synthesis technique introduced in [12] is used to design the suspension and drag-free controllers. In the following, for the sake of completeness, a brief description of the synthesis method is given. The interested reader can find a more detailed description in the referenced paper.

First of all, let us define a set of uncertain matrices with a given structure:

$$\mathbf{\Delta} := \{\Delta = \mathrm{diag}[I_{n_1}\otimes\Delta_1, \ldots, I_{n_g}\otimes\Delta_g, I_{n_{g+1}}\otimes\Delta_{g+1}, \ldots, I_{n_{g+d}}\otimes\Delta_{g+d}]:$$
$$\Delta_i = \Delta_i^T \in \mathbb{R}^{k_i\times k_i}\ \forall\, i\in\{1,\ldots,g\} \text{ and } \Delta_i \in \mathbb{C}^{k_i\times k_i}\ \forall\, i\in\{g+1,\ldots,g+d\}\} \tag{13}$$

where

$$y(s) \approx m_{\mathrm{TM}}^{-1}\{f_{\mathrm{TM}_x} + K_{xx}\underbrace{[S_{\mathrm{DF}}\Gamma_{\mathrm{DF}}(d_{\mathrm{SC}} + m_{\mathrm{TM}}^{-1}h_{IS}I_{\mathrm{TM}}(-T_{\mathrm{SUS}}d_{\mathrm{TM}} - T_{\mathrm{SUS}}/\Gamma_{\mathrm{SUS}}\eta_\phi)) - T_{\mathrm{DF}}\eta_x]}_{x} + K_{x\phi}\underbrace{[S_{\mathrm{SUS}}\Gamma_{\mathrm{SUS}}d_{\mathrm{TM}} - T_{\mathrm{SUS}}\eta_\phi}_{\phi}$$
$$+ h_{IS}I_{\mathrm{TM}}\underbrace{[-T_{\mathrm{SUS}}d_{\mathrm{TM}} - T_{\mathrm{SUS}}/\Gamma_{\mathrm{SUS}}\eta_\phi]}_{u_{\mathrm{SUS}}}\} \tag{12}$$

$$\sum_{i=1}^{g+d} n_i k_i = r$$

A set of uncertain stable transfer function matrices with structure Δ can be then defined as

$$\Pi_\Delta := \{\Delta(s) \in \mathcal{RH}_\infty : \Delta(s_0) \in \mathbf{\Delta} \quad \forall\ s_0 \in \bar{\mathbb{C}}_+, \|\Delta\|_\infty \le 1\} \tag{14}$$

Most linear time invariant closed loop systems subject to perturbations can be redrawn into the form depicted in Fig. 5a, where $\Gamma(s)$ is the known part of the plant partitioned consequently with the interconnection. In Fig. 5a, $\Delta(s) \in \Pi_\Delta$ represents a stable perturbation with r inputs and r outputs, whereas $K(s)$ is an internally stabilizing controller with p inputs and q outputs. The system is subject to the exogenous disturbances d and the control objective is measured in terms of the error signals e. The required performances of the closed loop system are included in the design by means of the diagonal frequency dependent performance weight

$$W \in \mathcal{W} := \{\mathrm{diag}_{i=1}^{n}[w_i] : w_i \in \mathcal{RH}_\infty\}$$

with $i = 1, \ldots, n$. The system achieves robust performance in the presence of uncertainty if

$$\|W\mathcal{F}_u(\mathcal{F}_l(G, K), \Delta)\|_\infty < 1 \tag{15}$$

where $\mathcal{F}_u(\cdot,\cdot)$ and $\mathcal{F}_l(\cdot,\cdot)$ are the lower and upper linear fractional transformations (see [25] for further details). The condition in Eq. (15) can be rewritten in terms of the supremum of the structured singular value (μ)

$$\sup_\omega \mu_\Delta\left[\begin{pmatrix} I & 0 \\ 0 & W(j\omega) \end{pmatrix}\mathcal{F}_l(\Gamma(j\omega), K(j\omega))\right] < 1 \tag{16}$$

where μ_Δ of a complex matrix M is defined as

$$\mu_{\mathbf{\Delta}}(M) = \frac{1}{\min\{\bar{\sigma}(\Delta) : \det(I - M\Delta) = 0, \Delta \in \mathbf{\Delta}_T\}} \tag{17}$$

and where

$$\mathbf{\Delta}_T := \{\mathrm{diag}(\Delta, \Delta_p) : \Delta \in \mathbf{\Delta}, \Delta_p \in \mathbb{C}^{m\times n}\}$$

denotes the total uncertainty structure with respect to which the structured singular value is computed (see Fig. 5b). However, the exact computation of this parameter is nonpolynomial hard [26] so that for common applications upper and lower bounds of μ_Δ are computed. A classical μ design problem with given performance and robustness specifications involves the search for a controller that minimizes the left-hand side of Eq. (16), that is, a controller that maximizes the size of the smallest possible uncertainty, Δ, that causes the loss of performance of the system. In other cases it may be desirable to maximize the performance of the system subject to the condition in Eq. (16). The control synthesis problem may then be reformulated as [27]

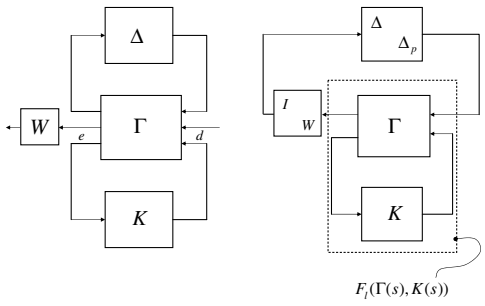

a) b)

Fig. 5 Generalized block interconnection for synthesis and analysis.

$$\max_W J(W)$$
$$\text{subject to } \min_{\mathcal{K}} \sup_\omega \mu_\Delta\left[\begin{pmatrix} I & 0 \\ 0 & W(j\omega) \end{pmatrix}\mathcal{F}_1(\Gamma(j\omega), K(j\omega))\right] < 1 \tag{18}$$

where $J(W)$ is an objective function that captures the performance preferences of the design and $\mathcal{K}$ is the set of all internally stabilizing controllers for the system $\mathcal{F}_l(\Gamma, K)$. In this case the optimization algorithm simultaneously synthesizes the controller and the weighting functions to maximize the closed loop performance of the system in some sense. A pointwise frequency solution of the optimization problem in Eq. (18) is proposed in [27] and a similar state space solution in [28] in the case of purely complex structured uncertainty.

In the following a brief description of the synthesis method capable to handle both parametric and complex uncertainties is given, detailing the definition of the objective function, $J(W)$, of the search space and showing the main steps in which the search procedure is divided.

A. Objective Function Definition

The objective function in Eq. (18) must be able to capture the performance preferences of the design that in common practice are reflected as gain requirements on the closed loop transfer functions. These gain requirements are usually handled by penalizing each output of the closed loop system with a weight, $w_i(j\omega)$, whose magnitude reflects the inverse of the desired specification bound. The objective function in Eq. (18) shall then represent a cumulative measure across frequency that reflects qualitatively the desired inverse performance weights shape.

Following the work in [27], let $[\omega_L, \omega_H]$ be a synthesis frequency range and $\upsilon_i(j\omega)$ be n given stable minimum phase transfer functions. Let us define

$$J(W) = \frac{1}{\int_{\log_{10}\omega_L}^{\log_{10}\omega_H} \sum_{i=1}^{n} \frac{1}{|w_i(j\omega)/\upsilon_i(j\omega)|^2}\,\mathrm{d}(\log_{10}\omega)} \tag{19}$$

The direction of steepest ascent in maximizing the function in Eq. (19) over any one weight $w_i(j\omega)$ at any one frequency ω in the frequency interval $[\omega_L, \omega_H]$ corresponds to the smallest ratio $|w_i(j\omega)/\upsilon_i(j\omega)|$. Consequently, the functions $\upsilon_i(j\omega)$ are called optimization directionalities because they can be specified so that they qualitatively direct the maximization where desired. Therefore $|\upsilon_i(j\omega)|$ should be set at a large value (respectively, small) at frequencies and in channel directions where the magnitude of the performance weight $w_i(j\omega)$ is required to be large (respectively, small) to capture the desired performance objectives. Defining an optimization directionality matrix as

$$\Upsilon(j\omega) := \mathrm{diag}(\upsilon_1(j\omega), \ldots, \upsilon_n(j\omega))$$

then (similar to [27]) the cost function in Eq. (18) can be defined as

$$J(W) = \frac{1}{\|\Upsilon W^{-1}\|^2_{[\omega_L,\omega_H]}}$$

where

$$\|X\|_{[\omega_L,\omega_H]} := \sqrt{\int_{\log_{10}\omega_L}^{\log_{10}\omega_H} \|X(j\omega)\|_F^2 \mathrm{d}(\log\omega)}$$

Note that only the argument of the optimization is of interest. Therefore the maximization of the cost can be replaced by the minimization of the reciprocal of $J(W)$ as will be seen in the next section.

B. Search Space Definition

In every optimization problem a crucial issue is the definition of the search space. First of all, since $\mu_\Delta(M) = \mu_\Delta(M^T)$, the

optimization problem in Eq. (18) can be equivalently rewritten in terms of the dual system

$$\min_{W\in\mathcal{W}} \|\Upsilon W^{-1}\|^2_{[\omega_L,\omega_H]} \quad \text{subject to}$$
$$\min_{K\in\mathcal{K}} \sup_{\omega} \mu_{\Delta_T}[\mathcal{F}_l(\Gamma,K)(j\omega)^T \operatorname{diag}[I_r, W(j\omega)]] < 1 \tag{20}$$

so that the inverses of the performance weights will appear in subsequent manipulations independently to form a convex constraint.

Now, to define an efficient solution algorithm, the robust performance constraint written in terms of μ_{Δ_T} will be replaced with a convex upper bound. Such an upper bound involves the definition of matrix scalings G and D allowed to vary in sets $\mathcal{D}$ and $\mathcal{G}$ that depend on the structure of the perturbation matrix Δ, that is,

$$\mathcal{D} := \{D = \operatorname{diag}[D_1 \otimes I_{k_1}, \ldots, D_g \otimes I_{k_g}, D_{g+1} \otimes I_{k_{g+1}}, \ldots, D_{g+d} \otimes I_{k_{g+d}}]: 0 < D_i = D_i^* \in \mathbb{C}^{n_i \times n_i}\}$$
$$\mathcal{G} := \{G = \operatorname{diag}[G_1 \otimes I_{k_1}, \ldots, G_g \otimes I_{k_g}, 0, \ldots, 0]: G_i = G_i^* \in \mathbb{C}^{n_i \times n_i}\} \tag{21}$$

The following lemma from [25] defines an upper bound on the structured singular value:

Lemma 1 (see [25]): Let $M \in \mathbb{C}^{r\times r}$ and $\Delta \in \mathbf{\Delta}$. Then

$$\mu_\Delta(M) \le \inf_{D\in\mathcal{D}, G\in\mathcal{G}} \min_{\beta}\{\beta: M^*DM + j(GM - M^*G) - \beta^2 D \le 0\} \tag{22}$$

This result can be reformulated in a more convenient way exploiting the result from the following lemma.

Lemma 2 (see [12]): Given a complex matrix $M \in \mathbb{C}^{r\times r}$, $D \in \mathcal{D}$, $G \in \mathcal{G}$, $\beta > 0$, and $\gamma \in [0, 1]$, then

$$\bar{\sigma}\left(\left(\frac{DMD^{-1}}{\beta} - jG\right)(I + G^2)^{-\frac{1}{2}}\right) \le \gamma \tag{23}$$

if and only if

$$\Omega(M, \hat{G}, \hat{D}, \beta, \gamma) := \begin{bmatrix} M^*\hat{D}M + j(\hat{G}M - M^*\hat{G}) - (\beta\gamma)^2\hat{D} & \sqrt{1-\gamma^2}\hat{G} \\ \sqrt{1-\gamma^2}\hat{G} & -\hat{D} \end{bmatrix} \le 0 \tag{24}$$

where $\hat{D} = D^*D \in \mathcal{D}$ and $\hat{G} = \beta D^*GD \in \mathcal{G}$.

By virtue of Lemma 2 an equivalent reformulation of the upper bound in Eq. (22) is

$$\Omega(M, G, D, \beta, 1) \le 0 \tag{25}$$

Note that by adding the fictitious uncertainty block $\Delta_p \in \mathbb{C}^{n\times n}$ to handle robust performance problems, the scaling matrices associated to the augmented uncertainty structure $\mathbf{\Delta}_T$ are $\operatorname{diag}[D, I_n]$, $D \in \mathcal{D}$ and $\operatorname{diag}[G, 0_n]$, $G \in \mathcal{G}$, where the last entry in the D scales has been normalized to unity. The following lemma provides an alternative upper bound on $\mu_{\Delta_T}[\mathcal{F}_l(\Gamma, K)(j\omega)^T \operatorname{diag}[I_r, W(j\omega)]]$.

Lemma 3 (see [12]): Given a closed loop system $\mathcal{F}_l(\Gamma, K) \in \mathcal{RH}_\infty$ and performance weights $W \in \mathcal{W}$. Then, $\forall\ \omega\ \exists\ D_\omega \in \mathcal{D}$, $G_\omega \in \mathcal{G}$, $\gamma_\omega \in [0, 1]$ and $\beta_\omega > 0$, such that

$$\Omega(\mathcal{F}_l(\Gamma, K)(j\omega)^T \operatorname{diag}[I_r, W(j\omega)], \operatorname{diag}[G_\omega, 0_n], \operatorname{diag}[D_\omega, I_n], \beta_\omega, \gamma_\omega) \le 0 \tag{26}$$

if and only if $\forall\ \omega\ \exists\ D_\omega \in \mathcal{D}$, $G_\omega \in \mathcal{G}$, $\gamma_\omega \in [0, 1]$ and $\beta_\omega > 0$, such that

$$\Omega(\mathcal{F}_l(\Gamma, K)(j\omega)^T, \operatorname{diag}[G_\omega, 0_n], \operatorname{diag}[D_\omega, I_n], \beta_\omega, \gamma_\omega) \le \operatorname{diag}[0_r, (\beta_\omega\gamma_\omega)^2(W_\omega - I_n), 0_{r+n}]$$

where $W_\omega = [W(j\omega)^* W(j\omega)]^{-1}$.

With the result from Lemma 3, and using the aforementioned upper bound of μ, the optimization problem in Eq. (18) is replaced by the following one:

$$\min_{W\in\mathcal{W}} \|\Upsilon W^{-1}\|^2_{[\omega_L,\omega_H]} \quad \text{such that}$$
$$\forall\ \omega\ \exists\ D_\omega \in \mathcal{D}, \quad G_\omega \in \mathcal{G} \quad \text{and} \quad \beta_\omega \in (0, 1) \text{ satisfying}$$
$$\Omega(\mathcal{F}_l(\Gamma, K)(j\omega)^T, \operatorname{diag}[G_\omega, 0_n], \operatorname{diag}[D_\omega, I_n], \beta_\omega, 1) \le \operatorname{diag}[0_r, \beta_\omega^2(W_\omega - I_n), 0_{r+n}] \tag{27}$$

When K is held fixed, the search space in Eq. (27) can be characterized by a set of linear matrix inequality constraints, uncoupled at each ω, and simultaneously quasi convex in D_ω, G_ω, W_ω, and β_ω. Hence, with K fixed in the inequality constraint, the minimization of the integral appearing in the cost function in Eq. (27) is equivalent to the minimization of the integrand on the continuum of frequencies. Therefore, under these assumptions, the cost function in Eq. (27) can be decoupled at each ω into $\|\Upsilon(j\omega)W(j\omega)^{-1}\|_F^2 = \operatorname{tr}(\Upsilon_\omega W_\omega)$, where we define the diagonal positive matrix

$$\Upsilon_\omega := \frac{\Upsilon(j\omega)^*\Upsilon(j\omega)}{\omega}$$

noting that the division by ω is necessary to take account of the logarithmic scale appearing in the cost function. A detailed description of the solution algorithm is given in [12].

V. Design Results

The synthesis technique outlined in the previous sections is here exploited to design the drag-free and suspension SISO controllers. First the top level requirement in Eq. (7) is broken down into specifications on the drag-free and suspension loops, respectively. Such specifications, given in the MBW, are shown in Table 3 and are derived from the closed loop measurement relation in Eq. (12) in which we substitute the worst case combination of parameters. Although the electrostatic forces directly compromise the accuracy level of the measurement, the actions exerted by the thruster actuators are not directly coupled to the measurement equation. Therefore, when high accuracy free fall is required, the instrument is operated in pure drag-free mode rather than in accelerometer mode [29]. This implies that a high bandwidth control is designed for the drag-free loop, whereas the gain of the suspension controller is reduced in the MBW. Moreover, as can be clearly seen from Figs. 2 and 3, the driving external disturbances appearing in Eq. (12) are the inertial sensor readout noise in the suspension loop and the thruster actuation noise in the drag-free loop. Therefore, the closed loop transfer functions related to these contributions in Eq. (12) are shaped directly in the SISO controllers design. As already pointed out in Sec. III, the simplified system is diagonal dominant and therefore the stability of the individual loops implies the stability of the overall system. This consideration allows one to tackle the design of the suspension and drag-free controllers separately once the coupling through h_{IS} is taken into account by properly writing the measurement equation from which the performance breakdown is derived.

Table 3 Specifications on the individual loops

Variable	Specification in the MBW
x	$3.05 \times 10^{-9}[1 + (\frac{f}{3\ \text{mHz}})^2]\ \frac{\text{m}}{\sqrt{\text{Hz}}}$
ϕ	$2.33 \times 10^{-6}[1 + (\frac{f}{3\ \text{mHz}})^2]\ \frac{\text{rad}}{\sqrt{\text{Hz}}}$
u_{SUS}	$2.33 \times 10^{-11}[1 + (\frac{f}{3\ \text{mHz}})^2]\ \frac{\text{rad}}{s^2\sqrt{\text{Hz}}}$

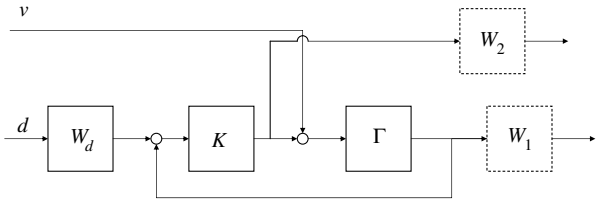

a) Drag-free controller design setup

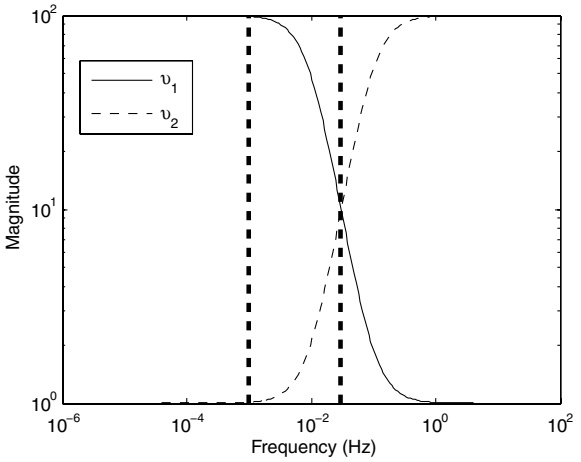

b) Optimization directionalities

Fig. 6 Input to the synthesis algorithm for drag-free design.

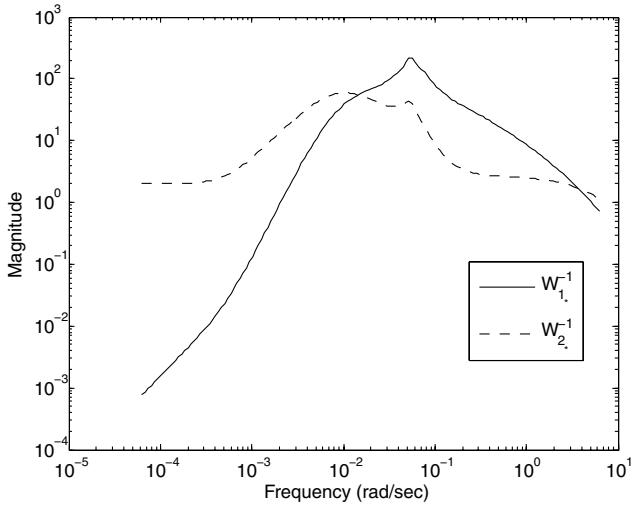

a) Optimal performance weights at the first iteration

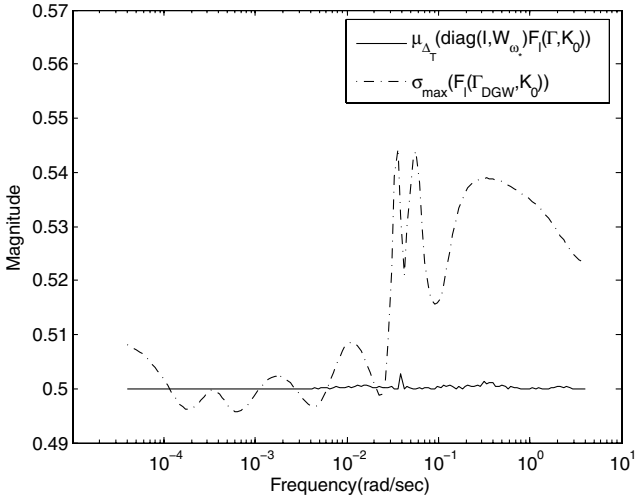

b) Maximum singular value and μ for the weighted closed loop system with the initial guess controller K_0

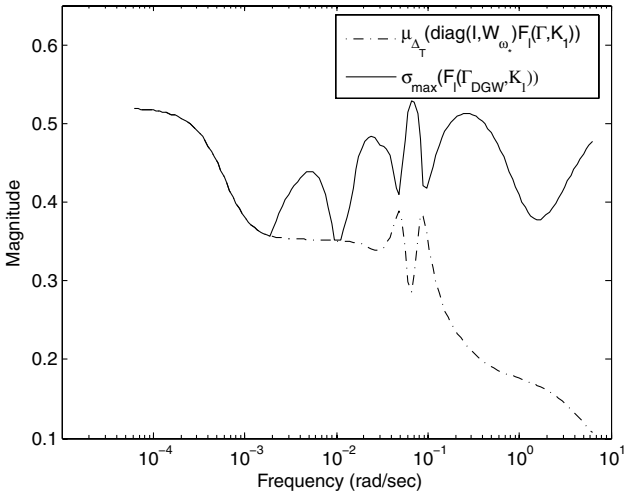

c) Maximum singular value and μ for the weighted closed loop system with the controller after the first redesign K_1

Fig. 7 Intermediate results after the first and second iterations.

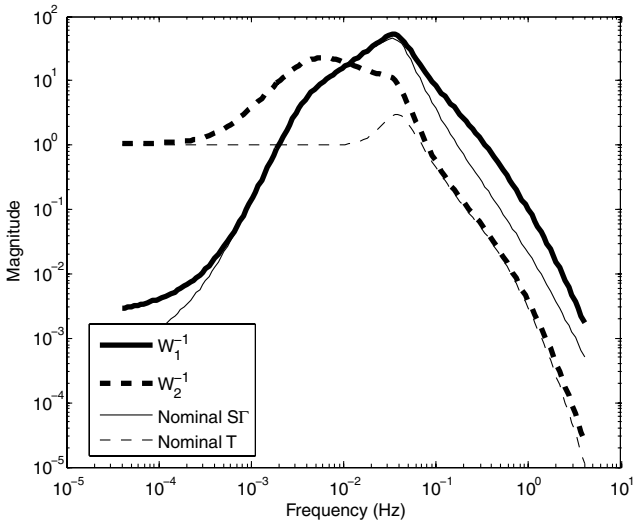

a) SΓ and *T* plots and corresponding performance weights in output to the synthesis algorithm

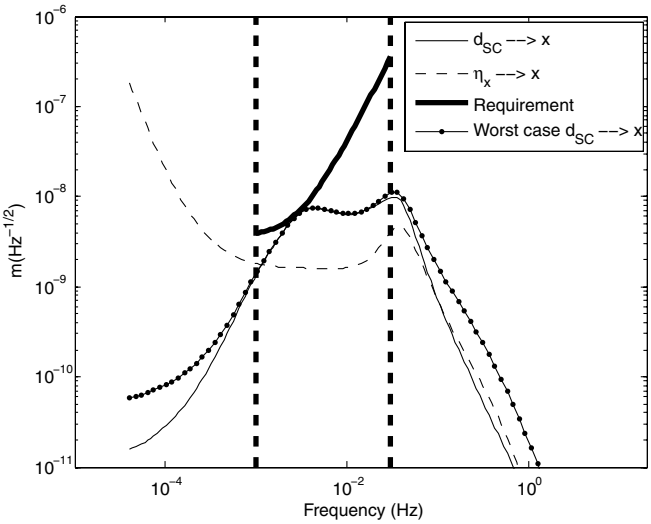

b) Closed loop response of the nominal drag-free SISO system

Fig. 8 Final results of the drag-free design procedure.

The inputs to the synthesis algorithm for the drag-free design are shown in Fig. 6. W_1 and W_2 shape $S\Gamma$ and T, respectively, and are automatically designed by the algorithm. The frequency range between (10^{-5} Hz, 10^{1} Hz) has been gridded with 150 points. As already mentioned above, this is the frequency range relevant for the system, covering from the inverse of the assumed experiment time to the controller sampling rate. The optimization directionalities in input to the drag-free control design are defined according to the following considerations. The highest source of noise entering in the drag-free loop is due to the thruster actuation system (see Fig. 2). Thruster noise appears directly in the measurement equation filtered by $S_{\mathrm{DF}}\Gamma_{\mathrm{DF}}$. To achieve the top level requirement in Eq. (7) it is thus highly desirable to have large attenuation of $S_{\mathrm{DF}}\Gamma_{\mathrm{DF}}$ in the measurement band. This requirement is introduced in the synthesis technique by simply setting a high level of the optimization directionality corresponding to W_1 in the MBW. Moreover, according to [7], to avoid the generation of command signals that exceed the capabilities of the FEEP actuator, an upper limit is posed on the control signal above the FEEP natural frequency. This is captured by setting high values of the optimization directionality that corresponds to the W_2 shape at high frequencies so that large attenuation of T_{DF} is required at frequencies above the MBW. Observe that the definition of the optimization directionalities presents fewer difficulties with respect to the direct synthesis of the weights W_1 and W_2 thus supporting the control designer in the choice of meaningful performance weights. For instance, the absolute magnitude of the optimization directionalities is irrelevant but only the shape and the relative magnitudes are taken into account by the search algorithm.

To illustrate the behavior of the algorithm as iterations proceed, consider Fig. 7 which gives plots of intermediate results after the first and the second iterations. At the beginning of the synthesis procedure an initial guess controller K_0 is designed with standard techniques. The definition of the initial robustness margin β_0 depends on the characteristics of the initial guess controller. In the drag-free control design the initial guess controller allows one to set the initial robustness margin to $\beta_0 = 0.5$. Moreover, the number of iterations required to reach the limit of performance is set to $N = 4$ (see [12] for a detailed definition of K_0, β_0). Figure 7a shows inverse magnitude pointwise plots of the optimal performance weights $W_{\omega_*}^{-1}$ in output to the analysis phase. In the Fig. 7b solid line, the structured singular value of the weighted closed loop system is computed, that is, $\mu_{\Delta_T}(\mathrm{diag}(I_r, W_{\omega_*})\mathcal{F}_l(\Gamma, K_0)(j\omega))$. Note that it approximately assumes the constant value of β_0 over frequency that means that W_{ω_*} represent the highest achievable performance given the robustness margin β_0. Then the robustness margin is relaxed $\beta_i = \beta_{i-1}(1+\epsilon)$ and suboptimal D_{ω_*} and G_{ω_*} scalings are computed. This allows one to have some more freedom in the approximation error when fitting the pointwise data. Then the optimal D_{ω_*}, G_{ω_*}, and W_{ω_*} weights are fitted to build the augmented plant Γ_{DGW}. In Fig. 7b, the dash-dotted

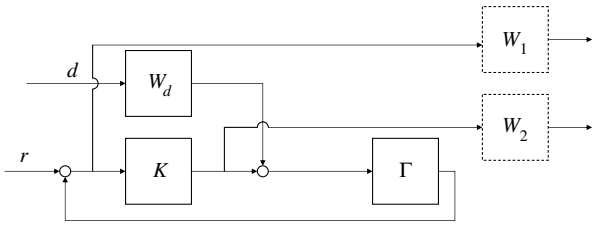

a) Suspension controller design setup

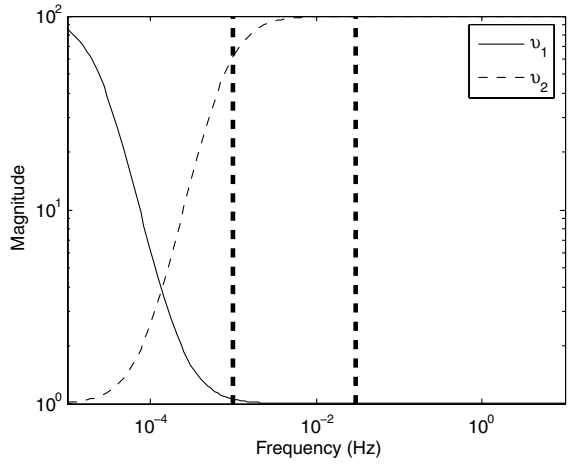

b) Optimization directionalities

Fig. 9 Input to the synthesis algorithm for suspension controller design.

line $\bar{\sigma}(\mathcal{F}_l(\Gamma_{DGW}, K_0))$ is plotted over frequency. The resulting value is not flat over frequency anymore because of the errors introduced by the fitting. Then an $\mathcal{H}_\infty$ synthesis technique is exploited to compute a new suboptimal controller K_1. In Fig. 7c the maximum singular value for the augmented closed loop system (solid line) and the structured singular value of the closed loop system (dash-dotted line) are displayed. In the regions where the structured singular value of the closed loop system reaches a value below β_0 a further improvement in performance can be achieved in the subsequent iteration. More details on the algorithm can be found in [12].

In Fig. 8 the results of the synthesis of the drag-free controller are presented. In Fig. 8a the pointwise magnitudes of the weights in output to the synthesis algorithm are shown together with the nominal closed loop transfer functions of interest. Comparing these results with the ones shown in Fig. 7a it is possible to conclude that the algorithm manages to reduce the magnitude of the corresponding weights in the desired frequencies range as the iterations proceed. Moreover, from a direct comparison between Fig. 6b and Fig. 8a it is possible to see how the optimized performance weights look different with respect to the optimization directionalities. This shows that the optimization synthesis technique automatically trades between performance requirement, robustness and limitations due to plant dynamics in order to maximize the cost defined in Sec. IV.A. It is important to highlight here that the design setup displayed in Fig. 6a is such that the performance weights multiply $S\Gamma$ and T rather than S and T. Therefore, the optimized performance weight W_1 and the associated closed loop transfer function have large magnitude before roll-off because of the large magnitude of Γ in the corresponding frequency range.

In Fig. 8b the magnitude plots of the nominal transfer function obtained by closing the drag-free loop in Fig. 4b with the designed drag-free controller are given. The bold line in this plot represents the requirement on the noise on the x axis obtained by the breakdown performed at the beginning of the design (see Table 3). In Fig. 8b the line with bullets marks represents an indication of the worst case transfer function from the thruster noise to the output of the drag-free loop (previously identified as a main design driver for the drag-free loop). This plot can be easily derived from the optimal performance weights in output to the synthesis algorithm and confirms that the system achieves the required level of performance even in the worst case. As a final remark, the designed controller after appropriate model reduction achieves a value of the SISO gain and phase margins of 6.12 dB and 35.9 deg, respectively.

The inputs to the synthesis algorithm for the suspension controller design are shown in Fig. 9. The performance weights W_1 and W_2 are automatically defined by the synthesis algorithm to shape S and $T\Gamma^{-1}$. In particular, the high magnitude of $\upsilon_1(j\omega)$ at low frequencies (below 1 mHz) implies that the optimization algorithm should

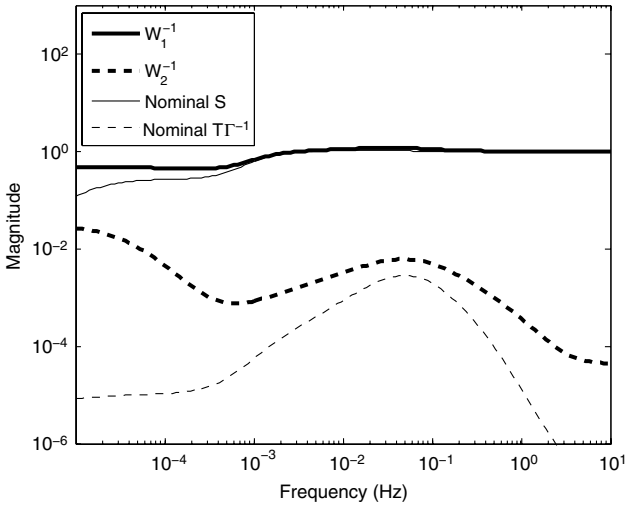

a) S and $T\Gamma^{-1}$ plots and corresponding performance weights in output to the synthesis algorithm

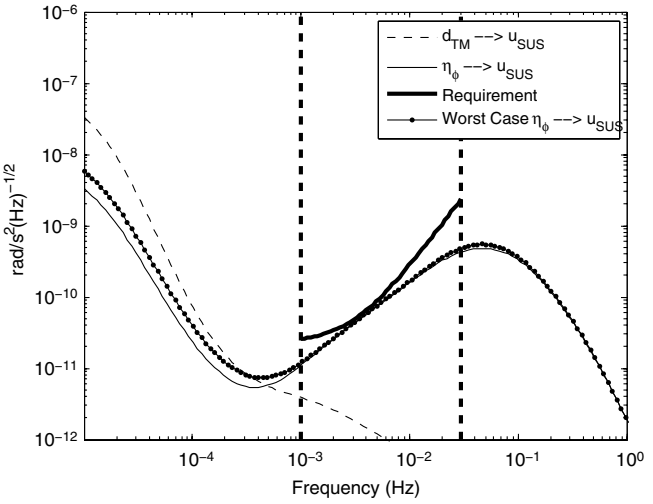

b) Closed loop response of the nominal suspension SISO system in terms of suspension control signal

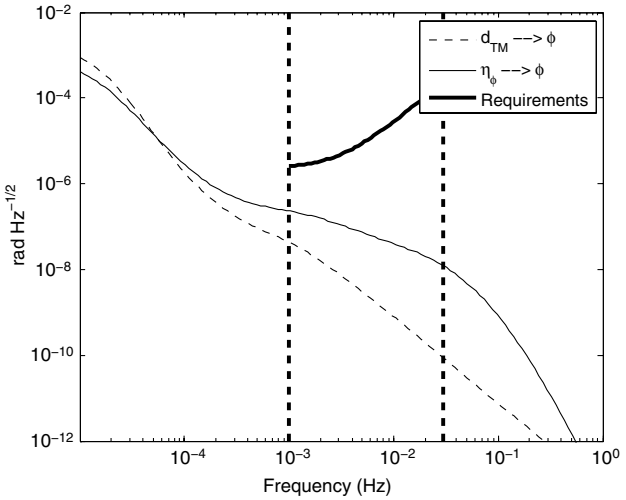

c) Closed loop response of the nominal suspension SISO system in terms of suspension loop output

Fig. 10 Final results of the suspension design procedure.

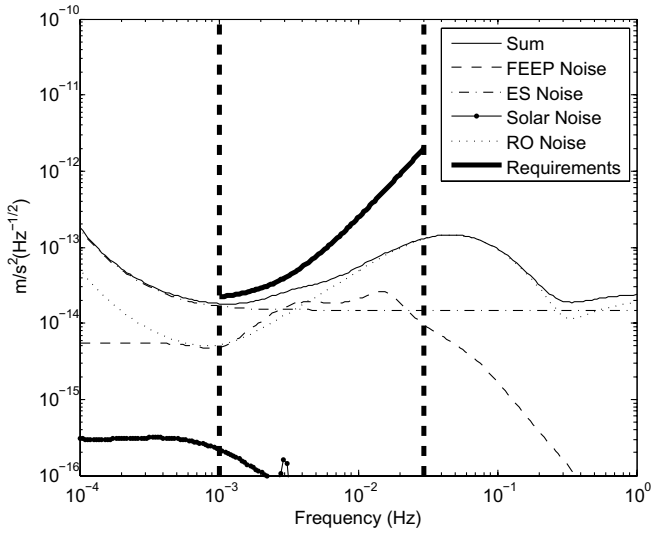

a) Absolute acceleration on the test mass along x for the nominal system

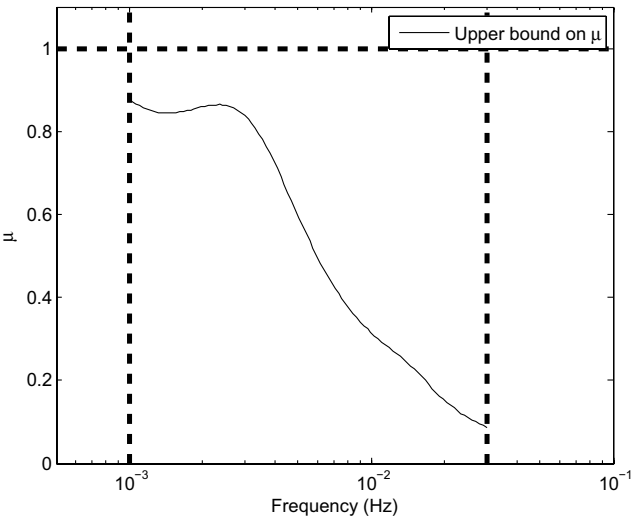

b) μ plot for the MIMO closed loop system

Fig. 11 MIMO closed loop robust performance analysis of the drag-free satellite. ES: electrostatic; RO: readout.

maximize W_1 at low frequencies. This is necessary to attenuate the disturbances in input to the suspension loop. On the other hand, the high magnitude of $v_2(j\omega)$ at high frequencies (above 1 mHz) states that the optimization problem should maximize as much as possible W_2 in the MBW. This will limit the effect of the inertial sensor readout noise on the suspension control force that couples directly with the measurement equation. The frequency range between (10^{-5}Hz, 10^{1}Hz) has been gridded with 150 points, the designed initial guess controller for the suspension loop allowed to set the initial robustness margin to $\beta_0 = 0.7$. Moreover, the number of iterations to reach the limit of robustness is set to $N = 4$.

The results in output to the synthesis algorithm are shown in Fig. 10. The algorithm converges after five iterations. In Fig. 10a the pointwise in frequency magnitudes of the inverses W_1 and W_2 in output to the synthesis algorithm are shown together with the nominal closed loop transfer functions S and $T\Gamma^{-1}$. The magnitude plot of each uncertain closed loop sensitivity function falls below the corresponding weight because robust performance is guaranteed. In Figs. 10b and 10c the response of the system obtained closing the suspension loop shown in Fig. 4b with the designed controller is displayed. In Fig. 10b the closed loop response from input disturbance and readout noise to control signal is presented. In this figure it is possible to see that the worst case transfer function from readout noise to actuation signal (previously identified as a main design driver for the suspension loop) clears the performance requirements, that is, the individual loop achieves the required level of robust performance. In Fig. 10c the closed loop frequency response from input disturbance and readout noise to the output ϕ of the suspension loop is given. In this case the requirements are met with some margin. Finally, the designed controller after appropriate model reduction achieves a value of the SISO gain and phase margin of 9.98 dB and 39.7 deg, respectively.

In Fig. 11 the nominal closed loop response (Fig. 11a) and the μ plot (Fig. 11b) of the fully coupled MIMO closed loop system are presented. These figures show, as expected, that the main performance goal in Eq. (7) is robustly achieved with margin.

As a final remark, the fastest poles of the drag-free and attitude controllers are given in Table 4. These are well below the assumed sampling frequency and therefore the controllers designed with the proposed method are suitable for a digital implementation.

VI. Verification with Time Domain Simulation

In this section, controllers designed with the method described in Secs. III and IV are tested against a more complex dynamical model describing a drag-free satellite.

To this end, an enhanced version of the drag-free satellite simulator presented in [30] has been used to assess the performance of the system by means of time domain simulations. The simulator integrates the nonlinear set of equations of motion of a drag-free satellite with physical characteristics consistent with the model described in Sec. II. In particular, diagonal inertia matrices are considered for both spacecraft and test mass both assumed to have approximately a cubic shape. The coupling between the test mass and the satellite is modeled by means of an uncertain stiffness matrix defined as follows:

$$K := \begin{bmatrix} K_{xx}I_3 + K_{xy}(E_3 - I_3) & K_{x\phi}E_3 \\ K_{\phi x}E_3 & K_{\phi\phi}I_3 + K_{\phi\theta}(E_3 - I_3) \end{bmatrix} \tag{28}$$

The numerical values of the additional uncertain parameters K_{xy} and $K_{\phi\theta}$ representing the stiffness cross couplings between the translational and rotational degrees of freedom, respectively, are given in Table 5.

The parameter h_{IS} is again used to model the direct electrostatic cross coupling between different test mass degrees of freedom. Command quantization has been included in the model with actuation resolutions consistent with those defined in Sec. II.B. Moreover, a FEEP maximum thrust of 150 μN (see [16]) and a suspension maximum torque of 1.0×10^{-10} N · m (see [21]) have been considered in the simulator. Finally, the filters used to describe the input noises associated with the actuators and the measurement noises are those given in Figs. 2 and 3 where the assumption on the disturbance torque due to the FEEP thrusters has been removed.

Table 4 Controllers fastest poles

Controller	Fastest pole, Hz
Drag free	0.39
Suspension	0.11

Table 5 Numerical value of additional stiffness parameters

Parameter	Nominal value	Uncertainty
K_{xy}	0.02×10^{-6} $\frac{\text{N}}{\text{m}}$	±50%
$K_{\phi\theta}$	0.3×10^{-9} $\frac{\text{N·m}}{\text{rad}}$	±50%

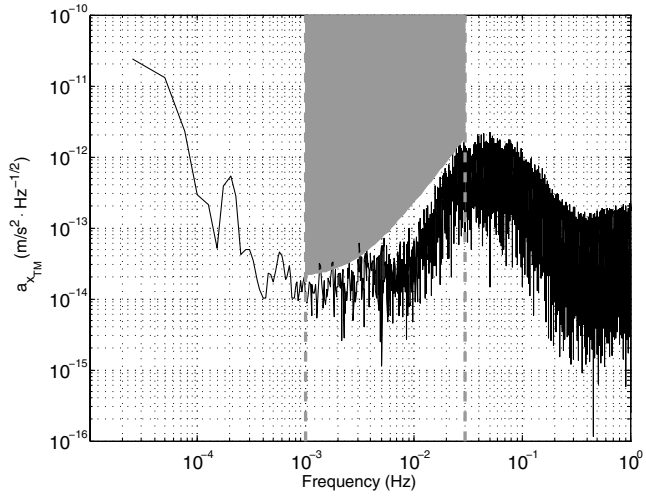

Fig. 12 PSD of the residual acceleration acting on the test mass.

Additional drag-free and suspension controllers have been synthesized to control the test mass position and attitude, respectively, in all 6 degrees of freedom. In addition, an attitude controller designed with conventional methods has been included in the loop to assess the performance of the overall system in a scenario consistent with the one defined in Sec. II. The control strategy suggested in [9] has been used to integrate the attitude controller and the drag-free and suspension controllers. According to this strategy, the test mass attitude is inertially fixed through the attitude controller and the spacecraft attitude is corrected through the drag-free loop.

The performance of the fully nonlinear system is tested against the requirement in Eq. (7). To assess the robustness of the system, a Monte Carlo analysis has been performed by checking the corners of the uncertain parameter space formed by $\{K_{xx}, K_{\phi x}, K_{x\phi}, K_{xy}, K_{\phi\phi}, K_{\phi\theta}, h_{IS}\}$. For each corner point of the parameter space, the PSD of the residual acceleration acting on the test mass in the x direction has been computed from a 5×10^4 s batch of time domain signal sampled at 10 Hz. The results of this computation for the case in which all the uncertain parameters are 1.5 times their nominal value (corresponding to a more unstable test mass-spacecraft coupling) are presented in Fig. 12. From this plot it is possible to see that the system achieves the required performance with the given combination of parameters. The same behavior was observed for all the combinations of parameters tested in the analysis providing evidence of the robustness of the system.

VII. Conclusions

This work addresses the problem of the design of a robustly performing decentralized controller for a high accuracy drag-free satellite with cubic test mass. First, an uncertain design plant set representative of the most modern drag-free satellites missions has been defined. The design plant was supposed to be uncertain and a performance requirement was imposed on the acceleration of the test mass along one of the two axes. An approximate uncertain plant set has been found relying upon the ν-gap metric and the measurement equation has been exploited to perform a worst case performance breakdown to derive requirements on the closed loop transfer functions of the individual loops. A recently developed iterative algorithm that performs an optimized tradeoff between achievable performance and limitations due to uncertainty or plant dynamics has been then considered to independently design the controller of each loop. The resulting design technique has shown to be easy and allows one to properly account for the uncertainty appearing in both the design plant and in the measurement equation while retaining the decentralized structure of the controller. To finally prove the results presented in this work, controllers designed with the proposed technique have been tested in a more realistic nonlinear simulation environment.

References

[1] Fichter, W., Gath, P., Vitale, S., and Bortoluzzi, D., "LISA Pathfinder Drag-Free Control System Implications," *Classical and Quantum Gravity*, Vol. 22, No. 10, 2005, pp. S139–S148. doi:10.1088/0264-9381/22/10/002

[2] Gath, W., Schulte, H., Weise, D., and Johann, U., "Drag Free and Attitude Control System Design for the LISA Science Mode," AIAA Paper 2007-6731, Aug. 2007.

[3] Sembely, X., Vaillon, L., and Vandermarq, O., "High Accuracy Drag-Free Control for The Microscope and Lisa Missions," *Proceedings of the 5th International Conference on Spacecraft Guidance, Navigation and Control*, European Space Agency, Noordwjik, The Netherlands, Oct. 2002.

[4] Jafry, Y., "Drag-Free Control for MiniSTEP," *Classical and Quantum Gravity*, Vol. 13, No. 11a, 1996, pp. A179–A184. doi:10.1088/0264-9381/13/11A/025

[5] Lange, B., "The Drag-Free Satellite," *AIAA Journal*, Vol. 2, No. 9, 1964, pp. 1590–1606. doi:10.2514/3.55086

[6] Chapman, D., Zentgraf, M., and Jafry, R., "Drag-Free Control Design Including Attitude Transition for the STEP Mission," *Proceedings of the 5th ESA International Conference on Spacecraft Guidance Navigation and Control*, European Space Agency, Noordwijk, The Netherlands, Oct. 2002.

[7] Bortoluzzi, D., Da Lio, M., Oboe, R., and Vitale, S., "Spacecraft High Precision Optimized Control for Free-Falling Test Mass Tracking in Lisa-Pathfinder Mission," *Advanced Motion Control*, IEEE, Piscataway, NJ, 2004, pp. 553–558.

[8] Fichter, W., Schleicher, A., Szerdahelyia, L., and Theil, S., "Drag-Free Control System for Frame Dragging Measurements Based on Cold Atom Interferometry," *Acta Astronautica*, Vol. 57, No. 10, 2005, pp. 788–799. doi:10.1016/j.actaastro.2005.03.070

[9] Fichter, W., Schleicher, A., and Vitale, S., "Drag-Free Control Design with Cubic Test Mass," *Lasers, Clocks and Drag-Free*, ZARM, University of Bremen, Germany, 2006.

[10] Bortoluzzi, D., Da Lio, M., Dolesi, R., Weber, W., and Vitale, S., "The LISA Technology Package Dynamics and Control," *Classical and Quantum Gravity*, Vol. 20, No. 10, 2003, pp. S227–S238. doi:10.1088/0264-9381/20/10/326

[11] Fichter, W., Schleicher, A., Bennani, S., and Wu, S., "Closed Loop Performance and Limitations of the LISA Pathfinder Drag-Free Control System," AIAA Paper 2007-6732, Aug. 2007.

[12] Pettazzi, L., and Lanzon, A., "Systematic Design of Optimal Performance Weight and Controller in Mixed-μ Synthesis," *8th IFAC World Congress*, Elsevier IFAC Publication, Oxford, England, U.K., July 2008, pp. 7814–7819.

[13] Canuto, E., "Drag-Free and Attitude Control for the GOCE Satellite," *Automatica*, Vol. 44, No. 7, 2008, pp. 1766–1780. doi:10.1016/j.automatica.2007.11.023

[14] Anderson, B., and Keller, J., "Discretization Techniques in Control Systems," *Control and Dynamic Systems*, Academic Press, New York, 1994, Vol. 66, pp. 47–112.

[15] Pettazzi, L., "Robust Controller Design for Drag-Free Satellites," Ph.D. Thesis, Faculty of Production Engineering, University of Bremen, 2008.

[16] Bindel, D., "FEEP Simulink Model for LISA Pathfinder End-2-End Simulator," ZARM TR S2-ZAR-TN-2007, Nov. 2005.

[17] Gollor, M., Weinberg, S., Boss, M., de la Cruz, F., Galantini, P., and Bourguignon, E., "Electric Propulsion Electronics Activities in Europe," AIAA Paper 2008-5284, July 2008.

[18] Maghami, P., O'Donnel, J., and Hsu, O., "Drag-Free Control Design for the ST7 Disturbance Reduction System Flight Experiment," AIAA Paper 2007-6731, Aug. 2007.

[19] Bortoluzzi, D., Carbone, L., Cavalleri, A., Da Lio, M., Dolesi, R., Hoyle, C., Hueller, M., Vitale, S., and Weber, W., "Measuring Random Force Noise for LISA Aboard the LISA Pathfinder Mission," *Classical and Quantum Gravity*, Vol. 21, No. 5, 2004, pp. S573–S579. doi:10.1088/0264-9381/21/5/028

[20] Gath, P., Fichter, W., Kersten, M., and Schleicher, A., "Drag Free and Attitude Control System Design for the LISA Pathfinder Mission," AIAA Paper 2004-5430, 2004.

[21] Ziegler, T., and Fichter, W., "Test Mass Stiffness Estimation for the LISA Pathfinder Drag-Free System," AIAA Paper 2007-6669, Aug. 2007.

[22] Schumaker, B., "Disturbance Reduction Requirements for LISA," *Classical and Quantum Gravity*, Vol. 20, No. 10, 2003, pp. S239–S253. doi:10.1088/0264-9381/20/10/327

[23] Criado, G., and Schleicher, A., "DFACS/LTP Interface Control Document," TR S2-ASD-ICD-2011, EADS-Astrium, Friedrichshafen, Germany, 2007.

[24] Vinnicombe, G., *Uncertainty and Feedback: $\mathcal{H}_\infty$ Loop Shaping and the ν-Gap Metric*, Imperial College Press, London, England, U.K., 2000.

[25] Zhou, K., and Doyle, J., *Essentials of Robust Control*, Prentice–Hall, Upper Saddle River, NJ, 1999, pp. 165–182.

[26] Braatz, R., Young, P., Doyle, J., and Morari, M., "Computational Complexity of μ Calculation," *IEEE Transactions on Automatic Control*, Vol. 39, No. 5, 1994, pp. 1000–1002. doi:10.1109/9.284879

[27] Lanzon, A., "Pointwise in Frequency Weight Optimization in μ-Synthesis," *International Journal of Robust and Nonlinear Control*, Vol. 15, No. 4, 2005, pp. 171–199. doi:10.1002/rnc.984

[28] Lanzon, A., and Cantoni, M., "On the Formulation and Solution of Robust Performance Problems," *Automatica*, Vol. 39, No. 10, 2003, pp. 1707–1720. doi:10.1016/S0005-1098(03)00184-5

[29] DeBra, D., "Drag-Free Control for Fundamental Physics Missions," *Advances in Space Research*, Vol. 32, No. 7, 2003, pp. 1221–1226. doi:10.1016/S0273-1177(03)90321-8

[30] Li, H., Theil, S., Pettazzi, L., Silas Guillerme, M., and Ni, W., "Dynamics Modeling and First Design of Drag-Free Controller for ASTROD I," *36th COSPAR Scientific Assembly*, Elsevier Publication, Oxford, England, U.K., July 2006.